

# Insights from Transient Absorption Spectroscopy into Electron Dynamics Along the Ga-Gradient in Cu(In,Ga)Se<sub>2</sub> Solar Cells

Yu-Han Chang, Romain Carron, Mario Ochoa, Carlota Bozal-Ginesta, Ayodhya N. Tiwari, James R. Durrant,\* and Ludmilla Steier\*

Cu(In,Ga)Se<sub>2</sub> solar cells have markedly increased their efficiency over the last decades currently reaching a record power conversion efficiency of 23.3%. Key aspects to this efficiency progress are the engineered bandgap gradient profile across the absorber depth, along with controlled incorporation of alkali atoms via post-deposition treatments. Whereas the impact of these treatments on the carrier lifetime has been extensively studied in ungraded Cu(In,Ga)Se<sub>2</sub> films, the role of the Ga-gradient on carrier mobility has been less explored. Here, transient absorption spectroscopy (TAS) is utilized to investigate the impact of the Ga-gradient profile on charge carrier dynamics. Minority carriers excited in large Cu(In,Ga)Se<sub>2</sub> grains with a [Ga]/([Ga]+[In]) ratio between 0.2–0.5 are found to drift-diffuse across  $\approx 1/3$  of the absorber layer to the engineered bandgap minimum within 2 ns, which corresponds to a mobility range of 8.7–58.9 cm<sup>2</sup> V<sup>-1</sup> s<sup>-1</sup>. In addition, the recombination times strongly depend on the Ga-content, ranging from 19.1 ns in the energy minimum to 85 ps in the high Ga-content region near the Mo-back contact. An analytical model, as well as drift-diffusion numerical simulations, fully decouple carrier transport and recombination behaviour in this complex composition-graded absorber structure, demonstrating the potential of TAS.

CuInSe<sub>2</sub> (CISe) lattice widens the bandgap from 1.04 eV<sup>[5,6]</sup> up to 1.68 eV<sup>[7]</sup> in pure CuGaSe<sub>2</sub>, the change affecting the conduction band and leaving the valence band largely unaffected.<sup>[8–10]</sup> Since 1994, several studies have focused on optimising device efficiency by adjusting the Ga-concentration profile in the CIGSe layer<sup>[3,11,12]</sup> nowadays reaching record device efficiencies surpassing 23%.<sup>[13]</sup> A double Ga-gradient profile (Ga-rich/Ga-poor/Ga-rich) is commonly implemented in high-efficiency CIGSe solar cells.<sup>[3,12,14]</sup> The gradient in the conduction band assists in driving electrons (minority carriers in p-type CIGSe) towards the space charge region (SCR) and the heterojunction with the n-type CdS layer.<sup>[15]</sup> The resulting decrease in electron density near the molybdenum (Mo) back contact has been shown to suppress recombination losses,<sup>[16–18]</sup> notably associated with interfacial recombination at the CIGSe/Mo junction,<sup>[14]</sup> thereby significantly increasing the device open-circuit voltage ( $V_{OC}$ ).<sup>[19–21]</sup>

## 1. Introduction

Bandgap engineering is employed in a wide range of commercialized and emerging photovoltaics such as Si,<sup>[1]</sup> CdTe,<sup>[2]</sup> Cu(In,Ga)Se<sub>2</sub> (CIGSe),<sup>[3]</sup> and perovskite<sup>[4]</sup> solar cells. State-of-the-art CIGSe solar cells make extensive use of a bandgap engineering approach, varying the [Ga]/([Ga]+[In]) ratio (GGI ratio) across the absorber thickness. The introduction of Ga into the

Optimisation of the CIGSe film thickness, composition and Ga-gradient profile has largely been carried out by monitoring improvements in device efficiency, with only limited knowledge of the underlying dynamics and diffusion of the minority carriers to the n-contact. In particular, minority carrier mobility and drift-diffusion times in high-efficiency CIGSe solar cells are important parameters to quantify performance losses in state-of-the-art devices. A number of studies report carrier mobility in CISe and CIGSe measured with a variety of techniques as summarised in **Table 1**. However, the reported mobility values show variations of several orders of magnitude. Furthermore, only a few studies investigated device-relevant Ga-graded CIGSe layers, instead, focusing on simpler, ungraded absorbers with poorer performance. Combining time-resolved photoluminescence (TRPL) spectroscopy and numerical simulations, Weiss et al. extracted minority carrier mobilities between 32 and 45 cm<sup>2</sup> V<sup>-1</sup> s<sup>-1</sup> in Ga-free CISe absorbers, however for back-graded CIGSe (GGI ratio increasing from 0 to 0.28 towards the back) only a lower limit of 8.3 cm<sup>2</sup> V<sup>-1</sup> s<sup>-1</sup> could be evidenced.<sup>[22]</sup> Kuciauskas et al. carried out TRPL studies on a typical Ga gradient device and estimated a minority carrier mobility of 55–230 cm<sup>2</sup> V<sup>-1</sup> s<sup>-1</sup> in the SCR near the CdS/CIGSe interface,<sup>[23]</sup> but did not address electron transport across the Ga-gradient towards the back contact region.

Though transient absorption spectroscopy (TAS) has been utilized in the fields of organic and hybrid organic–inorganic

Dr. Y.-H. Chang, C. Bozal-Ginesta, Prof. J. R. Durrant, Dr. L. Steier  
Department of Chemistry  
Imperial College London  
White City Campus, London W12 0BZ, UK  
E-mail: j.durrant@imperial.ac.uk; l.steier@imperial.ac.uk

Dr. R. Carron, Dr. M. Ochoa, Prof. A. N. Tiwari  
Laboratory for Thin Films and Photovoltaics  
Empa – Swiss Federal Laboratories for Materials Science and Technology  
Überlandstrasse 129, Dübendorf CH-8600, Switzerland

 The ORCID identification number(s) for the author(s) of this article can be found under <https://doi.org/10.1002/aenm.202003446>.

© 2021 The Authors. Advanced Energy Materials published by Wiley-VCH GmbH. This is an open access article under the terms of the Creative Commons Attribution License, which permits use, distribution and reproduction in any medium, provided the original work is properly cited.

DOI: 10.1002/aenm.202003446

**Table 1.** Electron/hole mobilities of CIGSe (and ClSe for comparison) extracted at room temperature from Hall effect, admittance spectroscopy, time-of-flight (ToF), terahertz (THz), time-resolved photoluminescence (TRPL), and transient absorption spectroscopy (TAS) measurements.

Technique	Material	Sample	GGI ratio	Mobility [ $\text{cm}^2 \text{V}^{-1} \text{s}^{-1}$ ]	Carrier	Reference
Hall	n-ClSe	Thin film	0	1–80	$e^-$	[35–38]
	n-ClSe	Single crystal	0	$\approx 1000$	$e^-$	[39–42]
	p-ClSe	Thin film	0	0.2–80	$h^+$	[36,37,43]
	p-ClSe	Single crystal	0	60–360	$h^+$	[39,42,44]
	p-CIGSe	Epitaxial thin film	0.031 to 1 <sup>a)</sup>	167–311	$h^+$	[45]
Admittance	p-CIGSe	Thin film	Not specified	4.08	$h^+$	[46]
THz	p-ClSe	Thin film	0	1000	$e^-$	[47]
ToF	p-CIGSe	Thin film	0.3	0.02–0.05	$e^-$	[48]
	p-CIGSe	Thin film	0.3	0.02–0.7	$h^+$	[49]
TR-PL	p-ClSe	Thin film	0	32–45	$e^-$	[22]
	p-CIGSe	Thin film <sup>b)</sup>	0.18 to 0.48 <sup>c)</sup>	55–230	$e^-$	[23]
	p-CIGSe	Thin film <sup>d)</sup>	0 to 0.28 <sup>c)</sup>	$\approx 8.3$	$e^-$	[22]
TAS	p-CIGSe	Thin film <sup>d)</sup>	0.20–0.67 <sup>c)</sup>	8.7–58.9	$e^-$	This study

<sup>a)</sup>Multiple samples with fixed GGI ratio; <sup>b)</sup>on SLG; <sup>c)</sup>Ga-gradient; <sup>d)</sup>RbF-NaF PDT.

perovskite photovoltaic materials to measure a wide range of charge carrier dynamics including recombination, charge carrier transfer and charge trapping,<sup>[24–29]</sup> only few TAS studies have been conducted in the CIGSe field. For example, Okano et al. elucidated the intraband charge carrier relaxation and localization processes in an ultra-thin film CIGSe absorber layer (film thickness around 200 nm) on femto-second to picosecond timescales.<sup>[30–32]</sup> Lee et al. utilized optical pump-terahertz probe spectroscopy to study the effect of Na and different fabrication methods of Zn(O,S) buffer layers on charge carrier lifetime in the SCR of CIGSe devices.<sup>[33,34]</sup>

Herein, we investigate minority carrier transport and recombination processes across the thickness of high-efficiency Ga-graded CIGSe films by use of broadband TAS on picosecond to nanosecond timescales. After removal of the back contact, charge carriers are excited at different depths in the Ga-graded CIGSe film by tuning the wavelength of the monochromatic excitation pulse. The charge carrier dynamics are probed by monitoring the change in optical absorption at various time and photon energies. We propose a kinetic model of competing carrier transport and recombination in a Ga-graded CIGSe film. Our measurements allow us to decouple both processes

and obtain the electron mobility across the bulk of the CIGSe film, outside the SCR, in the presence of a Ga-gradient with a GGI ratio varying from 0.5 to 0.2. In addition, a drift-diffusion simulation is employed to validate our results. Furthermore, we observed that the charge carrier lifetime is significantly reduced in regions with increased GGI, and that no charge transport is detected from the small-grained CIGSe region near the back interface.

## 2. Results and Discussion

The sample investigated is a typical Ga-graded CIGSe solar cell with a device efficiency >19% (**Figure 1a**) comprising of a 2.7  $\mu\text{m}$  thick *p*-type CIGSe absorber layer that is deposited on a Mo coated glass substrate and treated with NaF and RbF prior to being coated with *n*-type CdS and contacted via ZnO and Al:ZnO. The device structure is shown in **Figure 1b** and further fabrication details are provided in detail elsewhere.<sup>[50]</sup> The ratio of indium and gallium is adjusted through the course of CIGSe film evaporation leading to a characteristic Ga-gradient profile<sup>[51–53]</sup> shown in **Figure 1c** which is extracted from a depth

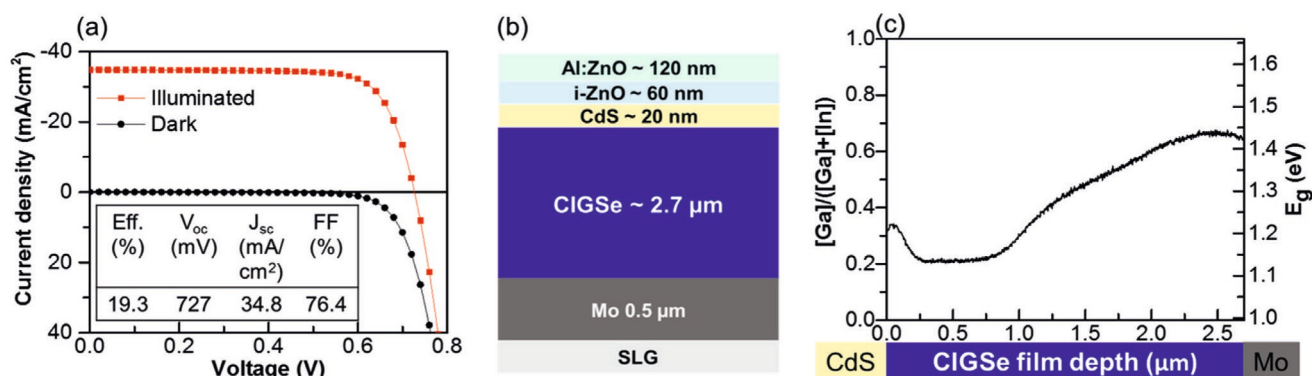


**Figure 1.** Cu(In,Ga)Se<sub>2</sub> solar cell properties. a)  $J$ - $V$  curve of CIGSe device measured under simulated sunlight (100  $\text{mW cm}^{-2}$ , 1 sun). b) Schematic of device structure showing CIGSe absorber layer grown on a Mo-coated soda lime glass (SLG) substrate and coated with 20 nm CdS, 60 nm i-ZnO and 120 nm Al:ZnO (AZO). c) Compositional depth profile from the SIMS measurements of the CIGSe film, showing the varying GGI ratio throughout the CIGSe film and the corresponding calculated bandgap energy,  $E_g$ .

profile secondary ion mass spectrometry (SIMS) measurement. From this composition profile the optical bandgap,  $E_g$ , is calculated from Equation 1

$$E_g^{\text{CIGSe}}(\text{GGI}(x)) = 1.004(1 - \text{GGI}(x)) + 1.663 \text{GGI}(x) - 0.033 \text{GGI}(x)(1 - \text{GGI}(x)) \quad (1)$$

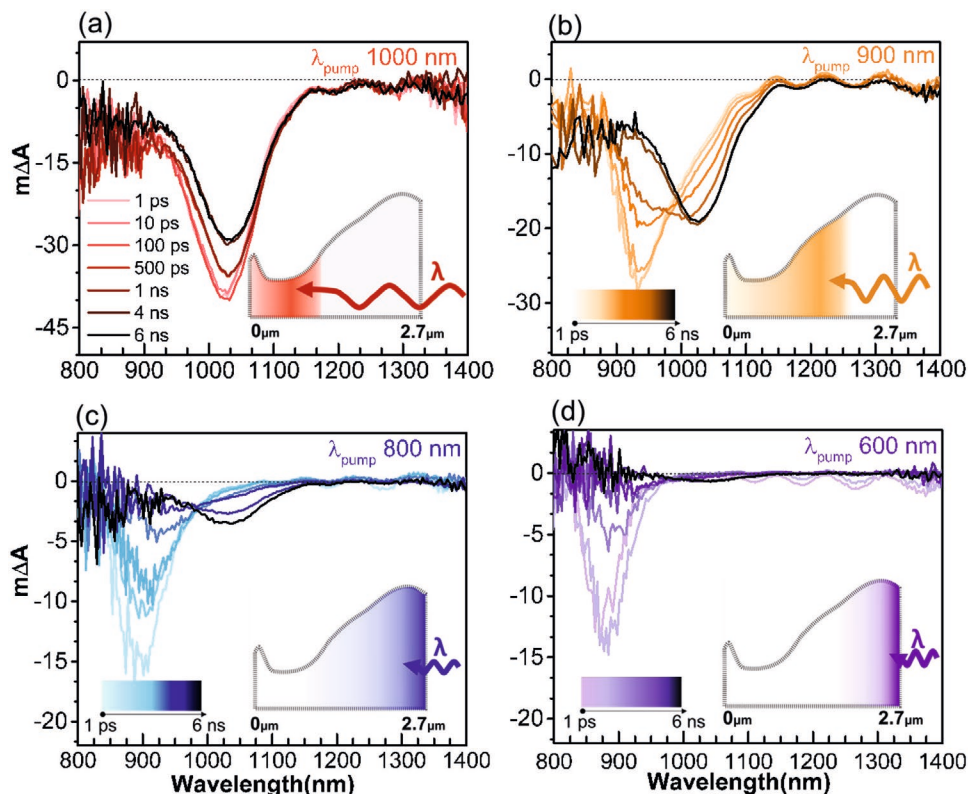
where the numbers were obtained previously from characterisation of a very comparable film.<sup>[54]</sup> Resulting values of  $E_g$  as a function of film depth are plotted in Figure 1c alongside the GGI ratio. The double Ga-gradient profile results in the formation of a bandgap minimum of 1.13 eV (GGI ratio of 0.2) about 2  $\mu\text{m}$  from the Mo-back contact, which is sandwiched by high bandgap CIGSe near the Mo back contact (1.44 eV, corresponding to a GGI ratio of 0.66–0.67) and at the CIGSe/CdS interface (1.22 eV, GGI ratio of 0.33–0.34). For TAS measurements the sample was prepared by delamination from the Mo back contact, onto a glass substrate using a transparent epoxy glue (see details in the Experimental Section).

Figure 2 shows time-resolved absorption spectra of the CIGSe/CdS/ZnO/AZO/epoxy/glass sample using varying excitation energies (600–1000 nm). The sample was excited from the high-GGI CIGSe side as shown in the insets in Figure 2, where the shaded area represents the charge carrier generation volume. The carrier generation profiles are shown in Figure S1, Supporting Information. For example, excitation with 1000 nm

(1.24 eV) laser light predominantly generates charge carriers in the energy notch (between 0–1.2  $\mu\text{m}$  from the CdS/CIGSe interface), whereas a 600 nm laser beam generates charge carriers in the high bandgap region within 200 nm from the back interface.

With 1000 nm excitation (Figure 2a), a negative  $\Delta A$  signal is observed with a minimum at 1025 nm (1.21 eV) shortly after excitation with 1000 nm laser light (i.e., within 1 ps). This signal essentially maintains its spectral signature during the entire time window of our measurement (from 1 ps to 6 ns), with only a modest decay in signal amplitude and a slight red-shift to a peak position of 1030 nm (1.20 eV). The energy of the photobleach (1.20 eV) coincides with the first derivative of the steady-state absorbance spectrum (Figure S2a, Supporting Information) and can hence be attributed to a band edge photobleach. We note that the steady-state photoluminescence spectrum of the same sample exhibits a  $\approx 70$  meV Stokes-shift relative to both these absorption features (Figure S2a, Supporting Information). An analogous Stokes-shift of  $\approx 70$  meV is also present in an ungraded CIGSe sample with a GGI ratio of 0.4 and no PDT treatment (Figure S2b, Supporting Information). These peak positions indicate that stimulated emission does not contribute significantly to the transient absorption signal.

In Figure 2b–d, we applied excitation pulses with increasingly higher photon energies (900, 800, and 600 nm). 1 ps after excitation we observe bleach signals centred at 936 nm (1.32 eV), 892 nm (1.39 eV), and 875 nm (1.42 eV), respectively. These



**Figure 2.** Ultrafast transient absorption spectra recorded at 1, 10, 100, 500 ps, 1, 4, and 6 ns after excitation of a Ga-gradient CIGSe sample using excitation wavelengths of a) 1000, b) 900, c) 800, and d) 600 nm. The light penetration depth of light impinging on the peeled-off Mo side and the resultant excitation volume in the CIGSe film are indicated in the inset in each spectrum. For (b), and (c), the pump fluence is 15.3 and 17.4  $\mu\text{J cm}^{-2}$  respectively, corresponding to  $7 \times 10^{13}$  photon  $\text{cm}^{-2}$ . For (a) and (d) the pump fluence is slightly different and the  $\Delta A$  signals are hence normalised to a photon flux of  $7 \times 10^{13}$  photons  $\text{cm}^{-2}$  absorbed.

signals are in agreement with the calculated bandgap energies in the respective excitation volumes. For example, the bandgap close to the back interface is between 1.42 and 1.44 eV (Figure 1c). With time, we observe a decay of the initial bleach, together with a rise of a 1025 nm bleach signal. By 6 ns, the initial bleach signals are fully decayed (Figure 2c,d), and only the 1025 nm bleach is observed for all excitation wavelengths. The rise of the 1025 nm bleach signal is thus a direct evidence of the kinetics of minority charge carrier transport from the higher bandgap excitation region to the low bandgap notch region, and the amplitude of the emerging 1025 nm bleach is a measure of the efficiency of this transport process. A study with excitation at either 355 nm or 700 nm from the glass/epoxy/AZO/ZnO/CdS/CIGSe side also shows that the initial photobleach shifted towards 1025 nm few hundred ps after excitation (Figure S3, Supporting Information). This observation further validates that the charge carriers generated in the high bandgap region move to the energy notch region, and not to the CdS/CIGSe interface. We note that for 900 nm excitation, the decay of the initial photobleach at 936 nm is coincident with a rise of the photobleach at 1025 nm. However for 800 and 600 nm excitation, a significant fraction of the initial photobleach decays faster and prior to growth of the 1025 nm photobleach, which we will discuss further below in our complete model of the CIGSe minority carrier dynamics.

## 2.1. Analytical Approach

Figure 3a illustrates a simple 3-level model that we use to explain and quantify the charge carrier dynamics in the Ga-graded CIGSe absorber. We use this model to understand the data obtained with 900 nm excitation. Electrons photo-generated in high GGI regions (denoted as the “H” level) undergo two competitive processes: 1) recombination and 2) drift-diffusion to the energy notch region. Kinetics for these two processes are given by Equations (2a) and (2b):

$$d[H]/dt = -(k_D + k_{rec}^H)[H] \quad (2a)$$

$$[H](t) = [H]_0 e^{-(k_D + k_{rec}^H)t} \quad (2b)$$

where  $k_{rec}^H$  and  $k_D$  represent the decay rate constants of recombination and drift-diffusion processes, and  $[H]_0$  the initial population of excited carriers in the high GGI region. The electrons that drift to the energy notch impact the population of carriers in the energy notch region (the “L” level) as per Equation (3a) and (3b):

$$d[L]/dt = -k_{rec}^L[L] + k_D[H] \quad (3a)$$

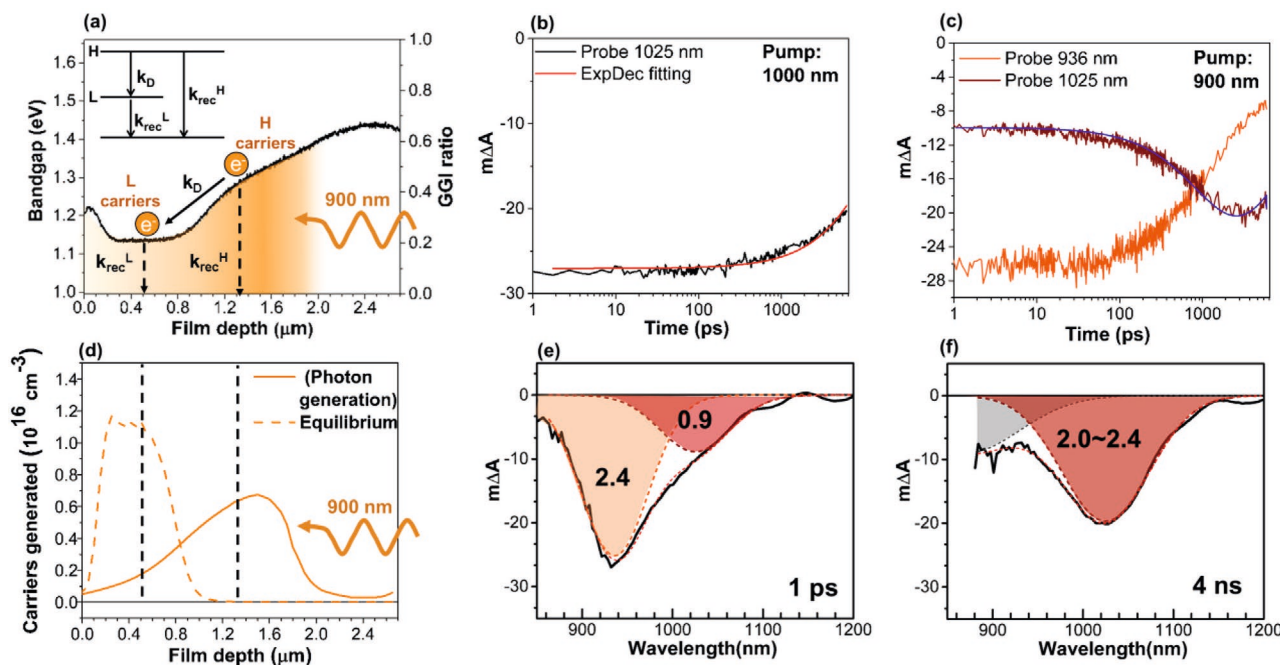


**Figure 3.** a) Schematic of proposed 3-level model for electrons in a Ga-graded CIGSe absorber excited with 900 nm light from the peeled-off Mo side.  $k_{rec}^L$  and  $k_{rec}^H$  represent the recombination processes of electrons at the energy notch (denoted L) and in the regions of high bandgap/high GGI ratio (denoted H).  $k_D$  represents the drift-diffusion process to the energy notch. b) TA decay kinetics probed at 1025 nm following a 1000 nm laser pulse from the peeled-off Mo side with a fluence of  $9.7 \mu\text{J cm}^{-2}$ . A single exponential function  $(\gamma = A \exp(-\frac{x}{t_1}), A = -0.027)$  is employed to fit this kinetic trace and the red thin line represents the fitting result. c) TA decay kinetics probed at 936 and 1025 nm following a 900 nm laser pulse from the peeled-off Mo side. The blue lines represent the fitting results. d) Charge carrier generation profile for 900 nm light impinging on the peeled-off CIGSe surface (Mo side) showing the carriers generated by a 900 nm laser pulse immediately after excitation (solid orange profile) and after diffusion happened such that equilibrium is reached (dashed orange profile). The dashed black lines show the mean position for each of the profiles. Deconvoluted integrated TAS spectra taken from Figure 2b at e) 1 ps and f) 4 ns, respectively.

$$[L](t) = \left( \frac{k_D}{k_D + k_{\text{rec}}^H - k_{\text{rec}}^L} [H]_0 + [L]_0 \right) e^{-k_{\text{rec}}^L t} - \frac{k_D}{k_D + k_{\text{rec}}^H - k_{\text{rec}}^L} [H]_0 e^{-(k_D + k_{\text{rec}}^H)t} \quad (3b)$$

Equation (3b) is the solution to the differential Equation (3a) and contains all necessary parameters to understand the kinetics in a Ga-graded CIGSe layer. It enables us to extract electron mobilities across the Ga-graded layer and understand the GGI-dependent recombination in high-quality CIGSe devices. In the following, we present a step-by-step approach to determine the required parameters.

The recombination in the energy notch  $k_{\text{rec}}^L$  can be obtained from excitation with 1000 nm pump laser energy (Figure 2a and Figure 3b). The high-energy level in our model remains empty ( $[H]_0 = 0$ ), as evident from Figure S1, Supporting Information. The model simplifies and  $k_{\text{rec}}^L$  becomes the only relevant parameter. By fitting the transient obtained with 1025 nm probe laser, we extract an electron lifetime in the notch  $1/k_{\text{rec}}^L = 19.1$  ns, as shown in Figure 3b.

To deconvolute  $k_D$  and  $k_{\text{rec}}^H$  we take advantage of the information provided by the spectra shown in Figure 2b and kinetics in Figure 3c. At 1 ps, the main peak is centred at 936 nm ( $\approx 1.32$  eV), but shows a tail towards lower energies (unlike the more symmetric bleach signal obtained when exciting with 1000 nm light as seen in Figure 2a). This tail originates from charge carriers photogenerated in the energy notch by the 900 nm pump pulse, as the charge carrier generation profile shown in Figure 3d indicates. Hence, by fitting the 1 ps spectrum with 2 Gaussian peaks centred at 936 and 1025 nm peaks and integrating the areas underneath, we estimate the amount of charge carriers generated in the higher GGI region to be 2.4 and in the energy notch to be 0.9, respectively (Figure 3e). With increasing time, the 936 nm signal decays whilst the 1025 nm signal grows, until reaching a plateau at approximately 4 ns (see 1025 nm kinetic trace in Figure 3c). The initial populations  $[H]_0 = -0.026$  and  $[L]_0 = -0.01$  are determined directly from the signal amplitudes of the 936 and 1025 nm kinetics at 1 ps, respectively, (Figure 3c). The number of electrons that successfully drifted to the energy notch can be estimated by fitting the 4 ns spectrum with a Gaussian peak centred at 1025 nm (Figure 3f). We note that a small residual signal at higher energies (illustrated as the grey area in Figure 3f) appears outside of the 1025 nm peak area. This is most likely due to the absorption processes within the bandgap of CIGSe (for example: deeper VB excitation), as this phenomenon is seen stronger in the case where the energy notch is directly excited (see Figure 2a). Consequently, the amount of charge carriers drifting to the energy notch is estimated to be 2.0–2.4, depending on the residual higher energy signal.

With the integrated areas, we can now define the ratio of generated carriers to those having drifted to the energy notch to be

$$\frac{k_D + k_{\text{rec}}^H}{k_D} = \frac{A_{936\text{nm},1\text{ps}}}{A_{1025\text{nm},4\text{ns}} - A_{1025\text{nm},1\text{ps}}} = 1.6-2.4 \quad (4)$$

which allows us to fit the 1025 nm kinetics (Figure 3c) with a modified Equation (3b) with  $k_D$  as the only fitting parameter.

Optimising the fit (see Section D in the Supporting Information for details), we obtain  $1/k_D = 1.918$  ns and calculate  $1/k_{\text{rec}}^H = 2.239$  ns for recombination in the graded CIGSe region with GGI ratio of  $\approx 0.5$ .

We note that TA kinetics showed no fluence dependency (see Section E in the Supporting Information), indicating a dominant monomolecular decay process. Considering the injection levels utilized (approximately  $4 \times 10^{16}$  to  $1 \times 10^{18}$   $\text{cm}^{-3}$  depending on fluence in the 900 nm case), it is surprising that the kinetics remain unchanged. Such behaviour may suggest a doping density of the CIGSe film higher than expected (about  $4 \times 10^{16}$   $\text{cm}^{-3}$ ), or/and charge carriers following Shockley–Read–Hall recombination, as observed in an air/CZTSSe/SiO<sub>2</sub>/Si film stack by Guglietta et al.<sup>[55]</sup>

The time constant of the drift-diffusion process,  $\tau_D = 1/k_D$ , can be employed to calculate the electron mobility in the Ga-graded CIGSe absorbers using Equation (5),

$$\mu = \frac{(\Delta x)^2}{\Delta \Phi \tau_D} \quad (5)$$

with  $\Delta x$  being the carrier travel distance,  $\Delta \Phi$  the corresponding potential change. To estimate the value of  $\Delta x$ , we performed optical transfer matrix method simulations (see Experimental Section). The generation profile of charge carriers in the CIGSe absorber was calculated using as input the bandgap profile shown in Figure 1c and the refractive indices of CIGSe reported elsewhere.<sup>[54]</sup> The resulting initial generation profiles are shown in Figure S1, Supporting Information, for various illumination wavelengths. The distribution of charge carriers at final time is assumed after diffusion takes place and is estimated by populating the bandgap profile according to the Boltzmann statistics, assuming a flat valence band condition. The corresponding distribution is shown in Figure 3d as the “equilibrium” case. The  $\Delta x$  value is taken as the difference between the mean values of the initial and equilibrium populations, that is, 796 nm, yielding a minority carrier mobility value of 23.3  $\text{cm}^2 \text{V}^{-1} \text{s}^{-1}$  in Ga-graded CIGSe. Taking into account error propagation from measurements and fittings, we estimate an electron carrier mobility ranging from 8.7–58.9  $\text{cm}^2 \text{V}^{-1} \text{s}^{-1}$  (see Section F, Supporting Information, for details).

## 2.2. Numerical Simulation Approach

The analytical approach used above is very simple, so for this proof-of-concept we decided to validate its results by numerically solving the drift-diffusion equations. In general, the TA signal evolution over time probes initially unoccupied states in the conduction band by tracking the carrier population affected by thermalization, transport, and recombination. Therefore, it is reasonable to relate the TA signal to a relative temporal carrier concentration modified by the three aforementioned mechanisms. To examine such mechanisms and support the analytical solution of the model, we performed numerical simulations by use of a drift-diffusion simulator (Sentaurus tool from Synopsys<sup>[56]</sup>). The tool self-consistently calculates the carrier distribution by solving the Poisson equation and the time-dependent transport and continuity equations. Because

the drift-diffusion simulator does not discriminate the energy distribution of carriers, we calculate at each absorber depth the electron distribution ( $N_E$ ) as a function of energy ( $E$ ), assuming that at each depth the energy of carriers is given by Boltzmann statistics (reasonable assumption for CIGSe), as indicated in Equation (6),

$$N_E(E) = N_{E,0}(E)e^{-E/kT} \quad (6)$$

where  $N_{E,0}$  corresponds to the local electron distribution calculated by Sentaurus. The carrier density is then integrated over the absorber depth as function of energy, using the bandgap profile obtained by SIMS (see Figure 1c).

An example of this calculation is shown in Figure 4a for a mobility of  $30 \text{ cm}^2 \text{ V}^{-1} \text{ s}^{-1}$ . As can be seen, already at 2 ns (orange line) most carriers have travelled from the energies associated to the back grading ( $E > 1.25 \text{ eV}$ ) towards the notch ( $E < 1.25 \text{ eV}$ ) consistent with Figure 2b, and supporting previous analysis. We now pay attention to the experimental TA decay kinetics and relate it to our simulations. We integrate the curve within intervals corresponding to the maximum values of  $N_E$  (at 1.145 eV and 1.35 eV  $\pm 10 \text{ meV}$  in Figure 4a) and normalize the data to evaluate the population changes as a function of the time for a wide range of carrier mobilities ( $10 \text{ cm}^2 \text{ V}^{-1} \text{ s}^{-1}$  to  $100 \text{ cm}^2 \text{ V}^{-1} \text{ s}^{-1}$ ). These kinetics are shown in Figure 4b,c illustrating the mobilities required to reproduce the TA signals are in the  $10 \text{ cm}^2 \text{ V}^{-1} \text{ s}^{-1}$  to  $\approx 60 \text{ cm}^2 \text{ V}^{-1} \text{ s}^{-1}$  range, being almost identical to the ones obtained analytically. Therefore, our numerical calculations fully support the analytical approach and results based on Equations (2)–(5).

Reported electron mobilities of polycrystalline CIGSe and CIGS vary five orders of magnitude ranging from  $0.02$  to  $1000 \text{ cm}^2 \text{ V}^{-1} \text{ s}^{-1}$ , as summarised in Table 1. Comparing the different experimental techniques, it is apparent that Time-of-Flight (TOF) measurements tend to measure mobility values on the lower edge of the above-mentioned range (typically  $0.02$ – $0.05 \text{ cm}^2 \text{ V}^{-1} \text{ s}^{-1}$ ).<sup>[48]</sup> In contrast, Tera-Hertz measurements provided an electron mobility of  $1000 \text{ cm}^2 \text{ V}^{-1} \text{ s}^{-1}$  in a stoichiometric CIGS thin film,<sup>[47]</sup> which is similar to the mobility for a CIGS single crystal. Due to the probing frequencies used, terahertz measurements access short-scale mobilities. Therefore, it gives a relatively high value compared to other methods, as it ignores grain boundary and some of the impurity scattering effects in the polycrystalline CIGSe. On the other hand, we obtain a mobility within a range of  $8.7$ – $58.9 \text{ cm}^2 \text{ V}^{-1} \text{ s}^{-1}$  in the large grain region (where  $\text{GGI} = 0.2$ – $0.5$ ), which is in good agreement with electron mobilities obtained from Hall measurements in n-type CIGS thin films ( $1$ – $80 \text{ cm}^2 \text{ V}^{-1} \text{ s}^{-1}$ )<sup>[35–38]</sup> and from TRPL studies for p-type CIGS ( $32$ – $45 \text{ cm}^2 \text{ V}^{-1} \text{ s}^{-1}$ )<sup>[22]</sup> and the space charge layer in Ga-graded CIGSe thin films ( $55$ – $230 \text{ cm}^2 \text{ V}^{-1} \text{ s}^{-1}$ ).<sup>[23]</sup>

### 2.3. Recombination at or Near the Back Interface

We now consider the dynamics of electrons generated close to the peeled-off Mo side, and in particular, the fast decay of the initial photobleach observed in Figures 2c,d.

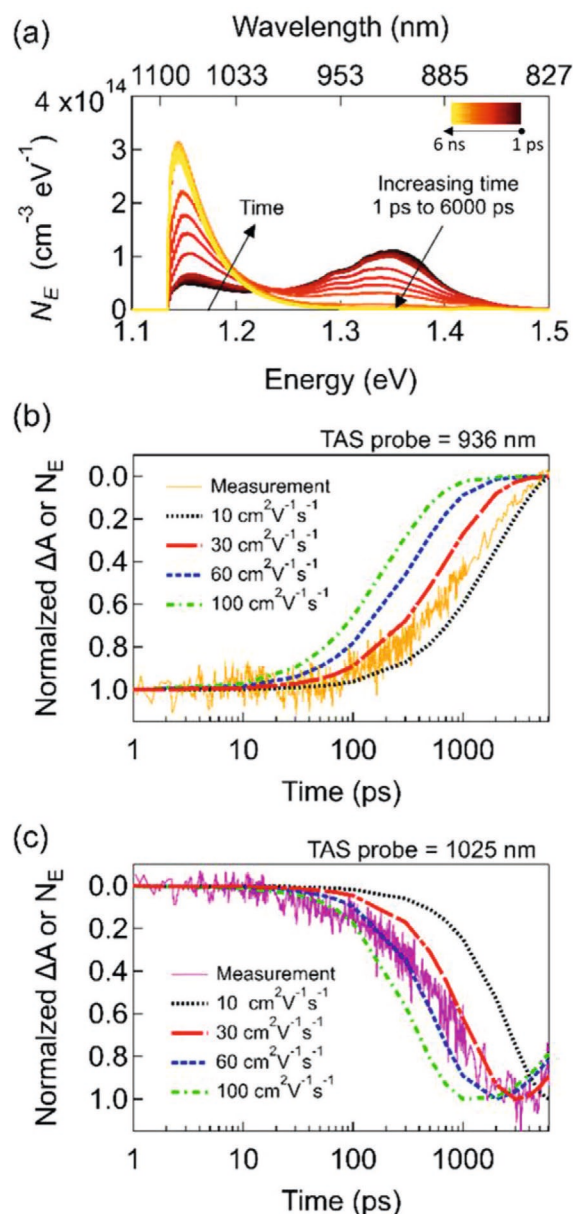


**Figure 4.** a) Electron distribution as a function of energy calculated at different times upon pump excitation of 900 nm for a mobility of  $30 \text{ cm}^2 \text{ V}^{-1} \text{ s}^{-1}$ . (b) and (c) illustrate the normalized TA kinetics (thin solid lines) and the normalized electron population for mobility in the range of  $10 \text{ cm}^2 \text{ V}^{-1} \text{ s}^{-1}$  to  $100 \text{ cm}^2 \text{ V}^{-1} \text{ s}^{-1}$  taken at energies corresponding to the peaks of (a), that is, b)  $1.145 \pm 0.01 \text{ eV}$  ( $1080 \pm 8 \text{ nm}$ ) and c)  $1.35 \pm 0.01 \text{ eV}$  ( $920 \pm 8 \text{ nm}$ ), respectively.

Figures 5a,b illustrate the transient absorption kinetics after 600 and 800 nm excitation. The 875 nm (Figure 5a) and 892 nm (Figure 5b) wavelengths correspond to the initial (1 ps) photobleach peak positions in the TAS spectra shown in Figures 2c,d, respectively, and therefore track the populations of carriers generated in the high bandgap region. As discussed above, the 1025 nm probe kinetics correspond to carriers in the energy notch region. As can be seen in Figures 5a,b, the decays of 875 and 892 nm signals are on the order of a 100 ps and

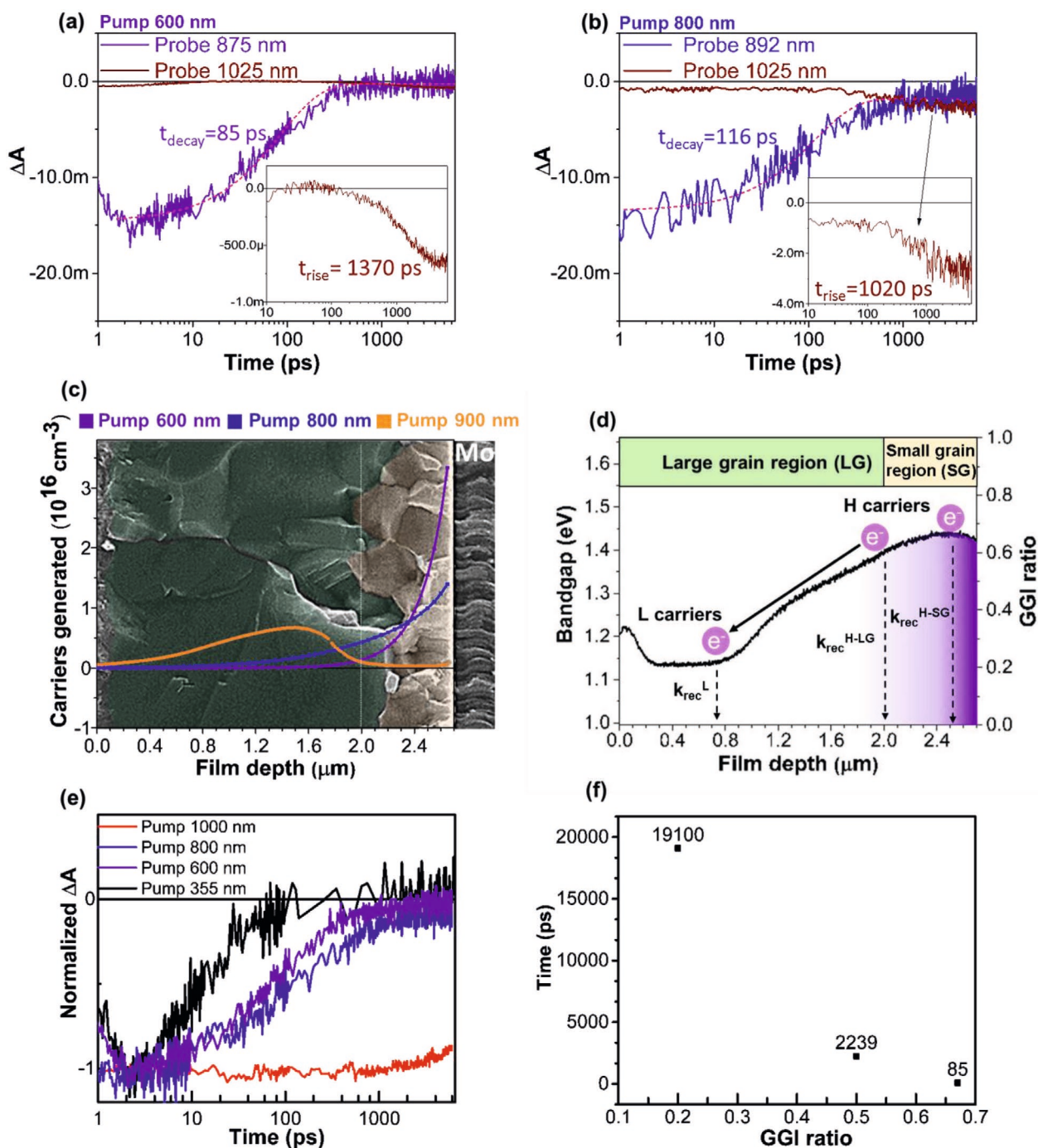


**Figure 5.** a) The TA kinetics probed at 875 and 1025 nm following 600 nm illumination and b) at 892 and 1025 nm following 800 nm illumination from the peeled-off Mo side. The red short dashed lines represent the fitting results. The insets show the 1025 nm traces more clearly. c) SEM cross-section image illustrating the morphology of the Ga-graded CIGSe absorber utilized for our TAS measurements. Simulated minority charge carrier concentration profiles in the Ga-graded CIGSe absorber directly after 600, 800, and 900 nm excitation from the peeled-off Mo side. d) Illustration of minority charge carrier dynamics in the Ga-graded CIGSe absorber after 600 nm illumination from the peeled-off Mo side.  $k_{\text{rec}}^{\text{L}}$ ,  $k_{\text{rec}}^{\text{H-LG}}$ , and  $k_{\text{rec}}^{\text{H-SG}}$  denote the charge recombination processes at the energy notch (region L), in the high bandgap regions exhibiting large grains (named as H-LG) and small grains (named as H-SG) respectively. e) Normalized transient absorption kinetics probed at 1025 nm for 1000 nm excitation (colour red), 892 nm for 800 nm excitation (colour blue), 875 nm for 600 nm excitation (colour purple), and 870 nm for 355 nm excitation (colour black) from the peeled-off Mo side. f) Extracted decay time constants in the regions of GGI = 0.2, 0.5, and 0.67.

hence significantly faster than the rise of the 1025 nm signal. Nonetheless, a small residual decay on the timescale of the 1025 nm rise is observed in both 875 and 892 nm traces.

To explain this observation, we turn to the analysis of the CIGSe film morphology. Figure 5c presents a typical cross-sectional SEM image of the Ga-graded CIGSe film. Large grains

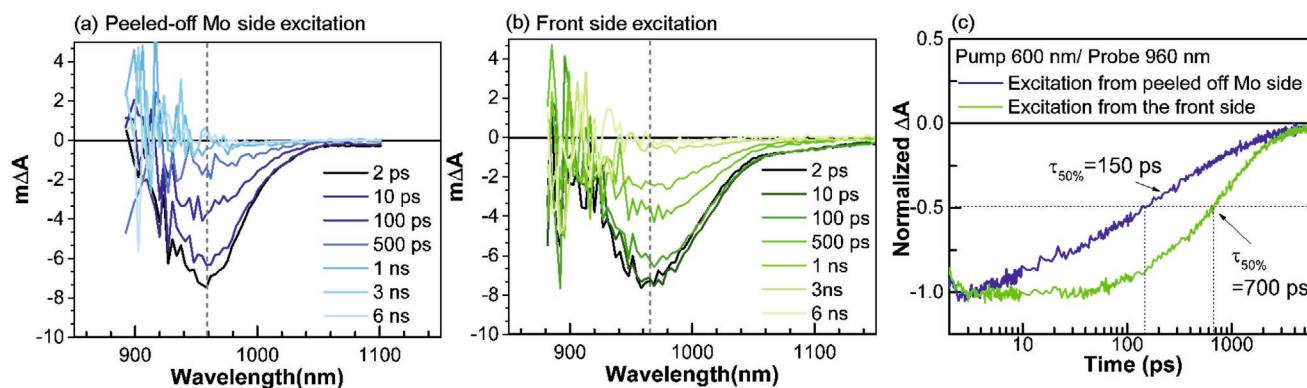


**Figure 6.** Transient absorption spectrum of an ungraded CIGSe sample with a GGI = 0.4 excited with 600 nm from the a) peeled-off Mo-side and b) the front side. c) Comparison of the TA kinetics probed at 960 nm in both excitation cases and their corresponding  $t_{50\%}$  decay times. Laser excitation fluence:  $2.5 \mu\text{J cm}^{-2}$ .

of CIGSe on the order of  $>2 \mu\text{m}$  dominate the device structure, however, significantly smaller grains ( $\approx 0.5 \mu\text{m}$ ) are visible near the Mo back interface (brownish shaded area in Figure 5c). In the following paragraphs, for the simplicity of description, we abbreviate the high GGI regions with large grains as “H-LG” and those with small grains as “H-SG”. From our charge generation profiles (overlaid curves in Figure 5c), it is seen that 600 nm laser light impinging on the sample from the peeled-off Mo side, generates charge carriers mostly in the H-SG region. 800 nm laser light, is also significantly absorbed in the H-SG region but shows a more evenly distributed absorption profile extending further into the H-LG region.

We hypothesise that the fast decay in Figures 5a,b represents charge carrier recombination in the H-SG region, whereas the slower 1025 nm rise signal stems only from charge carriers generated in the H-LG region drift-diffusing to the energy notch.

To quantify the amount of H-LG and H-SG electrons generated initially, we first consider the 800 nm excitation case: the 1 ps TA spectrum is fitted with two peaks: 1) 892 nm, which corresponds to the H-SG electrons, and 2) 936 nm, which corresponds to the H-LG electrons (Figure S10, Supporting Information). The fitting result shows that only 29% of the carriers generated are H-LG electrons. In the 600 nm excitation case, only 5% of H-LG carriers are generated (Figure S11, Supporting Information). Analysis of the optical simulations yields comparable estimates: only 38% and 8% of the photon flux is absorbed after the first 500 nm for 800 and 600 nm excitation, respectively. The 1025 nm rise amplitude in the 800 nm excitation case is also  $\approx 6$  times larger than in the 600 nm excitation case, consistent with this analysis of a varying ratio of H-LG to H-SG carriers in different excitation volumes.

Hence, we can conclude that electrons generated close to the back interface with Mo in the small grain region (H-SG,  $\text{GGI} > 0.5$ ) are all lost to recombination and do not contribute to the device performance. This is consistent with previous studies investigating the impact of different GGI ratios on grain size, recombination and overall device performance: a report summarizing the electronic defects of CIGSe and CGSe previously studied by photoluminescence, admittance, and photocurrent spectroscopies showed that deep recombination centres exist when the GGI ratio exceeds 0.5.<sup>[57]</sup> In fact, the grain size itself is also influenced by the GGI ratio: it has been shown that Ga atoms have a low diffusivity

and tend to accumulate at CIGSe/Mo interface where they restrain grain growth.<sup>[58]</sup> Fan et al. designed four different Ga gradient profiles and found that a separated layer consisting of small grains was formed close to CIGSe/Mo interface in all four samples.<sup>[59]</sup> Lundberg et al. observed a correlation of a smaller grain size and a decrease in cell performance which was attributed to increased grain boundary recombination.<sup>[60]</sup> We also observe a clear correlation between higher GGI ratio and faster recombination time in our experiments. Figures 5e,f illustrate the decay kinetics probing at the initial bleach position with 355, 600, 800, and 1000 nm excitation energies. It is obvious that the kinetics decayed much faster with increasing excitation energies, leading to a faster recombination time. As discussed in the literature, our observations could be explained by an increased surface recombination or/and increased number of bulk defects in regions with a higher GGI ratio.

To elucidate the role of surface recombination, we excited a CIGSe sample exhibiting a homogenous grain size and GGI ratio ( $=0.4$ ) with 600 nm excitation energy from the peeled-off Mo side and the front side (Figure 6). The results show a 4.7-fold decrease of charge carrier lifetime when exciting closer to the peeled-off Mo side with a large air-exposed CIGSe surface. The TA decay is about  $10\times$  slower when illuminating the sample from the CdS-passivated side. Therefore, surface recombination certainly contributes to the decreased lifetime of charge carriers generated closer to the peeled-off Mo side. This effect is possibly promoted by surface oxidation arising from air exposure. In a functional device with Mo back contact, interfacial recombination is likely to be even more pronounced,<sup>[22]</sup> such that charge transport from the small grain region to the energy notch is also unlikely.

### 3. Conclusion

In summary, we accessed the minority charge carrier dynamics in a CIGSe absorber by TAS. We observed the competition between recombination and transport kinetics at different depths of the NaF + RbF treated Ga-graded CIGSe layer. We developed an analytical model and quantified the electron mobility to a range of  $8.7\text{--}58.9 \text{ cm}^2 \text{ V}^{-1} \text{ s}^{-1}$ , specifically in the large grain region where  $\text{GGI} = 0.2\text{--}0.5$ . Within the large grain region, charge carrier recombination depends on the GGI ratio (i.e., 2–3 ns where  $\text{GGI} = 0.5$  versus  $\approx 19$  ns where  $\text{GGI} = 0.2$ ). More elaborated, but

more difficult to implement numerical drift-diffusion simulations confirmed the validity of the simple 3-level model and confirmed the values obtained. Charge carrier recombination also appears highly dependent on the morphology. When grain size is rather small (i.e.,  $\leq 0.5 \mu\text{m}$ ) then recombination lifetimes decrease to values significantly lower than 1 ns (i.e.,  $\approx 100 \text{ ps}$ ). Our results show that carriers generated within 500 nm from the back contact are unlikely to diffuse to the front electrode due to the combined influence of bulk and interface recombination. Improving the back contact in CIGSe solar cells is a major challenge in the efforts of reaching higher device efficiencies. We will discuss the effects of alkali PDTs on competing charge carrier dynamics and the resulting device efficiency in a subsequent work. We note, however, that in devices and modules showing pinholes and other fabrication defects, an H-SG region will likely always be prone to undergo surface oxidation which can result in recombination rates as fast as a few hundreds of picoseconds. The outcomes of our study provide important insights on the operation within the entire CIGSe device that can guide future solar cell design and show that TAS is a powerful tool for direct observation of minority carrier dynamics, often difficult to track with other techniques.

## 4. Experimental Section

**J–V Measurements:** Solar cells were characterized by current-voltage (J–V) measurements at 25 °C under a simulated AM 1.5G spectrum in an ABA-class solar simulator.

**SIMS Measurements:** The compositional depth profile was acquired using a time-of-flight SIMS (ION-TOF GmbH TOF SIMS5) with  $\text{O}^{2+}$  for sputtering and  $\text{Bi}^+$  for analyzing.

**TAS Measurements:** Seed pulses (800 nm,  $< 100 \text{ fs}$  width) were generated at a repetition rate of 1 kHz by a Ti:Sapphire regenerative amplifier (Spectra-Physics Solstice, Newport Corporation). The laser beam was then split and passed through an optical parametric amplifier (TOPAS, Light Conversion) coupled to a frequency mixer (NIRUVIS, Light Conversion) to generate the pump pulses of the specific excitation wavelength (355, 600, 800, 900, and 1000 nm in this study). The 800 nm probe pulses were directed to a mechanical delay stage followed by a Ti:Sapphire crystal to generate a white light continuum. The pump (modulated at 500 Hz) and the broadband near-infrared ( $\approx 850\text{--}1350 \text{ nm}$ ) probe were focused onto a  $\approx 0.5 \text{ mm}^2$  spot on the sample and the resulting change in absorption was transmitted to a commercially available femtosecond transient absorption spectrometer (HELIOS, Ultrafast Systems). Note that  $\Delta A = 0$  means that the optical absorption was unchanged as compared to prior to the excitation pulse. The intensity of the excitation laser beam was adjusted with neutral density filters.

**CIGSe Sample Preparation for TAS Measurements:** To access the detection of charge carrier dynamics at the back interface in such a thick strongly absorbing film, the CIGSe sample was detached from the Mo back contact as follows. First, the glass side of the CIGSe solar cell was glued with transparent epoxy adhesive (3M Scotch-Weld DP100) to a 2 mm thick glass substrate for mechanical support. Second, a small droplet of the transparent epoxy adhesive was deposited on top of the CIGSe solar cell. Third, a second glass substrate was then used to cover the epoxy droplet and placed starting with an angle to avoid air enclosure. Last, a small weight ( $\approx 100 \text{ g}$ ) was placed carefully on the assembly and kept for one day. Afterwards, the sandwiched sample was heated to 50 °C for 1 h and allowed to cool down before the top glass piece was pulled from the bottom piece, thereby, peeling off a circle of the solar cell stack from the Mo back contact. The resulting sample architecture used in our transient absorption (TAS) measurements was shown in the main manuscript (Figure 1b) with laser pulses impinging either on the peeled-off CIGSe side or the glass/epoxy/AZO/ZnO/CdS side.

We note that small cracks were present in the delaminated CIGSe layers due to deformation of the epoxy. The cracks isolate rather large

CIGSe regions, of lateral dimensions in the range of 10's  $\mu\text{m}$  to several mm. The distance between cracks was significantly larger than the lateral diffusion length of charge carriers. The diffusion length in CIGS was about 4–5  $\mu\text{m}$ , but was effectively lowered to  $< 2 \mu\text{m}$  when restricted to early times dynamics (assuming  $\mu = 60 \text{ cm}^2 \text{ V}^{-1} \text{ s}^{-1}$ ). Therefore, we expect no significant effect of the cracks on the dynamics of charge carriers. This was supported by the results from Feurer et al.<sup>[9]</sup> and Weiss et al.,<sup>[22]</sup> where no negative impact on the TRPL decay lifetimes of the peeled-off CIGSe and CIGSe samples was found.

**Optical TMM Simulations:** Optical transfer matrix method simulations were performed similarly as described in detail elsewhere.<sup>[54]</sup> The optical propagation in the multilayer was implemented in the tmm python package. The multilayer was as follows: SLG, epoxy, ZnO:Al, ZnO, CdS, CIGSe. The CIGSe absorber was subdivided in 50 nm-thick layers with GGI composition ratio discretized from the depth profile presented in Figure 1c. The refractive indices were taken from the results published by Carron et al.<sup>[54]</sup>

**Drift-Diffusion Simulations:** Drift-diffusion simulations were carried out with Sentaurus tool from Synopsis. The structure corresponds to the CIGSe absorber discretized in 10 nm layers with GGI ratio as in Figure 1c. The CIGSe refractive indices as function of GGI were taken from the results published by Carron et al.<sup>[54]</sup> A monochromatic source of 900 nm has been used as excitation resembling low injection conditions. Current boundary conditions were assumed for transient simulations. A uniform carrier lifetime of 20 ns has been set, as determined for the notch region in the experimentally probed timescales. We noticed minor modifications to our results by assuming GGI-dependent carrier lifetime properties, as determined experimentally in the manuscript. The rest of the material parameters for CIGSe can be found elsewhere.<sup>[61]</sup>

## Supporting Information

Supporting Information is available from the Wiley Online Library or from the author.

## Acknowledgements

Y.-H.C. Chang thanks the Ministry of Education of Taiwan for her Ph.D. scholarship, and Dr. Michael Sachs for fruitful discussions on TA data. J.R.D. would like to thank the UKRI Global Challenge Research Fund project SUNRISE (EP/P032591/1). L.S. acknowledges funding from the European Research Council (H2020-MSCA-IF-2016, Grant No. 749231). This work received financial support from the Swiss State Secretary for Education, Research and Innovation (SERI) under contract number 17.00105 (EMPIR project HyMet). The EMPIR programme is co-financed by the Participating States and by the European Union's Horizon 2020 research and innovation programme.

## Conflict of Interest

The authors declare no conflict of interest.

## Data Availability

Data underlying this article can be accessed on Zenodo at [10.5281/zenodo.4419686], and used under the Creative Commons Attribution 4.0 International licence.

## Keywords

charge carrier recombination, CIGS solar cells, composition gradient, minority carrier mobility, transient absorption spectroscopy

Received: October 31, 2020

Revised: December 22, 2020

Published online: January 14, 2021

- [1] K. Masuko, M. Shigematsu, T. Hashiguchi, D. Fujishima, M. Kai, N. Yoshimura, T. Yamaguchi, Y. Ichihashi, T. Mishima, N. Matsubara, T. Yamanishi, T. Takahama, M. Taguchi, E. Maruyama, S. Okamoto, *IEEE J. Photovoltaics* **2014**, *4*, 1433.
- [2] J. D. Poplawsky, W. Guo, N. Paudel, A. Ng, K. More, D. Leonard, Y. Yan, *Nat. Commun.* **2016**, *7*, 1.
- [3] A. Chirilă, S. Buecheler, F. Pianezzi, P. Bloesch, C. Gretener, A. R. Uhl, C. Fella, L. Kranz, J. Perrenoud, S. Seyrling, R. Verma, S. Nishiwaki, Y. E. Romanyuk, G. Bilger, A. N. Tiwari, *Nat. Mater.* **2011**, *10*, 857.
- [4] K. T. Cho, S. Paek, G. Grancini, C. Roldán-Carmona, P. Gao, Y. Lee, M. K. Nazeeruddin, *Energy Environ. Sci.* **2017**, *10*, 621.
- [5] J. E. Jaffe, A. Zunger, *Phys. Rev. B* **1984**, *29*, 1882.
- [6] S. Wagner, J. L. Shay, P. Migliorato, H. M. Kasper, *Appl. Phys. Lett.* **1974**, *25*, 434.
- [7] M. Saad, H. Riazi, E. Bucher, M. C. Lux-Steiner, *Appl. Phys. A: Mater. Sci. Process.* **1996**, *62*, 181.
- [8] S. Wei, A. Zunger, *J. Appl. Phys.* **1995**, *78*, 3846.
- [9] S.-H. Wei, S. B. Zhang, A. Zunger, *Appl. Phys. Lett.* **1998**, *72*, 3199.
- [10] J. Bekaert, R. Saniz, B. Partoens, D. Lamoen, *Phys. Chem. Chem. Phys.* **2014**, *16*, 22299.
- [11] A. M. Gabor, J. R. Tuttle, M. H. Bode, A. Franz, A. L. Tennant, M. A. Contreras, R. Noufi, D. G. Jensen, A. M. Hermann, *Sol. Energy Mater. Sol. Cells* **1996**, *41–42*, 247.
- [12] M. A. Contreras, J. Tuttle, A. Gabor, A. Tennant, K. Ramanathan, S. Asher, A. Franz, J. Keane, L. Wang, R. Noufi, *Sol. Energy Mater. Sol. Cells* **1996**, *41–42*, 231.
- [13] “Best Research-Cell Efficiency Chart | Photovoltaic Research | NREL,” <https://www.nrel.gov/pv/cell-efficiency.html>, (accessed: n.d.).
- [14] M. Murata, D. Hironiwa, N. Ashida, J. Chantana, K. Aoyagi, N. Kataoka, T. Minemoto, *Jpn. J. Appl. Phys.* **2014**, *53*, 04ER14.
- [15] J. Song, S. S. Li, C. H. Huang, O. D. Crisalle, T. J. Anderson, *Solid-State Electron.* **2004**, *48*, 73.
- [16] Y. Ando, S. Ishizuka, S. Wang, J. Chen, M. M. Islam, H. Shibata, K. Akimoto, T. Sakurai, *Jpn. J. Appl. Phys.* **2018**, *57*, 08RC08.
- [17] T. Dullweber, G. Hanna, U. Rau, H. W. Schock, *Sol. Energy Mater. Sol. Cells* **2001**, *67*, 145.
- [18] T. Feurer, P. Reinhard, E. Avancini, B. Bissig, J. Löckinger, P. Fuchs, R. Carron, T. P. Weiss, J. Perrenoud, S. Stutterheim, S. Buecheler, A. N. Tiwari, *Prog. Photovoltaics* **2017**, *25*, 645.
- [19] T. Feurer, B. Bissig, T. P. Weiss, R. Carron, E. Avancini, J. Löckinger, S. Buecheler, A. N. Tiwari, *Sci. Technol. Adv. Mater.* **2018**, *19*, 263.
- [20] T. Dullweber, O. Lundberg, J. Malmström, M. Bodegård, L. Stolt, U. Rau, H. W. Schock, J. H. Werner, *Thin Solid Films* **2001**, *387*, 11.
- [21] M. Topič, F. Smole, J. Furlan, *J. Appl. Phys.* **1996**, *79*, 8537.
- [22] T. P. Weiss, B. Bissig, T. Feurer, R. Carron, S. Buecheler, A. N. Tiwari, *Sci. Rep.* **2019**, *9*, 1.
- [23] D. Kuciauskas, J. V. Li, M. A. Contreras, J. Pankow, P. Dippo, M. Young, L. M. Mansfield, R. Noufi, D. Levi, *J. Appl. Phys.* **2013**, *114*, 154505.
- [24] A. A. Bakulin, A. Rao, V. G. Pavelyev, P. H. M. Van Loosdrecht, M. S. Pshenichnikov, D. Niedzialek, J. Cornil, D. Beljonne, R. H. Friend, *Science* **2012**, *335*, 1340.
- [25] M. Sachs, R. S. Sprick, D. Pearce, S. A. J. Hillman, A. Monti, A. A. Y. Guilbert, N. J. Brownbill, S. Dimitrov, X. Shi, F. Blanc, M. A. Zwiijnenburg, J. Nelson, J. R. Durrant, A. I. Cooper, *Nat. Commun.* **2018**, *9*, 4968.
- [26] A. Marchioro, J. Teuscher, D. Friedrich, M. Kunst, R. Van De Krol, T. Moehl, M. Grätzel, J. E. Moser, *Nat. Photonics* **2014**, *8*, 250.
- [27] K. Gao, Z. Zhu, B. Xu, S. B. Jo, Y. Kan, X. Peng, A. K.-Y. Jen, *Adv. Mater.* **2017**, *29*, 1703980.
- [28] H. Löslein, T. Ameri, G. J. Matt, M. Koppe, H. J. Egelhaaf, A. Troeger, V. Sgobba, D. M. Guldi, C. J. Brabec, *Macromol. Rapid Commun.* **2013**, *34*, 1090.
- [29] J. Horn, I. Minda, H. Schwoerer, D. Schlettwein, *Phys. Status Solidi* **2018**, *256*, 1800265.
- [30] M. Okano, Y. Takabayashi, T. Sakurai, K. Akimoto, H. Shibata, S. Niki, Y. Kanemitsu, *Phys. Rev. B* **2014**, *89*, 195203.
- [31] M. Okano, H. Hagiya, T. Sakurai, K. Akimoto, H. Shibata, S. Niki, Y. Kanemitsu, *Appl. Phys. Lett.* **2015**, *106*, 181903.
- [32] M. Okano, L. Q. Phuong, Y. Kanemitsu, *Phys. Status Solidi* **2015**, *252*, 1219.
- [33] W. J. Lee, D. H. Cho, J. H. Wi, H. J. Yu, W. S. Han, J. M. Bae, J. Park, Y. D. Chung, *ACS Appl. Energy Mater.* **2018**, *1*, 522.
- [34] W. J. Lee, D. H. Cho, J. H. Wi, W. S. Han, Y. D. Chung, J. Park, J. M. Bae, M. H. Cho, *J. Phys. Chem. C* **2015**, *119*, 20231.
- [35] L. L. Kazmerski, M. S. Ayyagari, F. R. White, G. A. Sanborn, *J. Vac. Sci. Technol.* **1976**, *13*, 139.
- [36] O. Tesson, M. Morsli, A. Bonnet, V. Jousseau, L. Cattin, G. Massé, *Opt. Mater.* **1998**, *9*, 511.
- [37] S. M. Firoz Hasan, M. A. Subhan, K. M. Mannan, *Opt. Mater.* **2000**, *14*, 329.
- [38] R. D. L. Kristensen, S. N. Sahu, D. Haneman, *Sol. Energy Mater.* **1988**, *17*, 329.
- [39] T. Irie, S. Endo, S. Kimura, *Jpn. J. Appl. Phys.* **1979**, *18*, 1303.
- [40] S. M. Wasim, A. Noguera, *Phys. Status Solidi* **1984**, *82*, 553.
- [41] L. Essaleh, S. M. Wasim, J. Galibert, *J. Appl. Phys.* **2001**, *90*, 3993.
- [42] P. M. Gorley, V. V. Khomyak, Y. V. Vorobiev, J. González-Hernández, P. P. Horley, O. O. Galochkina, *Sol. Energy* **2008**, *82*, 100.
- [43] N. G. Dhere, M. Cristina Lourenço, R. G. Dhere, L. L. Kazmerski, *Sol. Cells* **1986**, *16*, 369.
- [44] S. M. Wasim, *Sol. Cells* **1986**, *16*, 289.
- [45] D. J. Schroeder, J. L. Hernandez, G. D. Berry, A. A. Rockett, *J. Appl. Phys.* **1998**, *83*, 1519.
- [46] S. Paul, R. Lopez, I. L. Repins, J. V. Li, *J. Vac. Sci. Technol., B: Nanotechnol. Microelectron.: Mater., Process., Meas., Phenom.* **2018**, *36*, 022904.
- [47] C. Strothkämper, A. Bartelt, R. Eichberger, C. Kaufmann, T. Unold, *Phys. Rev. B* **2014**, *89*, 115204.
- [48] S. A. Dinca, E. A. Schiff, W. N. Shafarman, B. Egaas, R. Noufi, D. L. Young, *Appl. Phys. Lett.* **2012**, *100*, 103901.
- [49] S. A. Dinca, E. A. Schiff, B. Egaas, R. Noufi, D. L. Young, W. N. Shafarman, *Phys. Rev. B* **2009**, *80*, 235201.
- [50] T. P. Weiss, S. Nishiwaki, B. Bissig, R. Carron, E. Avancini, J. Löckinger, S. Buecheler, A. N. Tiwari, *Adv. Mater. Interfaces* **2018**, *5*, 1701007.
- [51] A. M. Gabor, J. R. Tuttle, D. S. Albin, M. A. Contreras, R. Noufi, A. M. Hermann, *Appl. Phys. Lett.* **1994**, *65*, 198.
- [52] S. Seyrling, A. Chirilă, D. Güttler, F. Pianezzi, P. Rossbach, A. N. Tiwari, *Thin Solid Films* **2011**, *519*, 7232.
- [53] P. Reinhard, F. Pianezzi, L. Kranz, S. Nishiwaki, A. Chirilă, S. Buecheler, A. N. Tiwari, *Prog. Photovoltaics* **2015**, *23*, 281.
- [54] R. Carron, E. Avancini, T. Feurer, B. Bissig, P. A. Losio, R. Figi, C. Schreiner, M. Bürki, E. Bourgeois, Z. Remes, M. Nesladek, S. Buecheler, A. N. Tiwari, *Sci. Technol. Adv. Mater.* **2018**, *19*, 396.
- [55] G. W. Guglietta, K. R. Choudhury, J. V. Caspar, J. B. Baxter, *Appl. Phys. Lett.* **2014**, *104*, 253901.
- [56] Synopsys, “Sentaurus Device User Guide.” Version P-2019.3 **2019**.
- [57] C. Spindler, F. Babbe, M. H. Wolter, F. Ehré, K. Santhosh, P. Hilgert, F. Werner, S. Siebentritt, *Phys. Rev. Mater.* **2019**, *3*, 90302.
- [58] H. H. Sung, D. C. Tsai, Z. C. Chang, B. H. Kuo, Y. C. Lin, T. J. Lin, S. C. Liang, F. S. Shieu, *Surf. Coat. Technol.* **2014**, *259*, 335.
- [59] Q. Fan, Q. Tian, H. Wang, F. Zhao, J. Kong, S. Wu, *J. Mater. Chem. A* **2018**, *6*, 4095.
- [60] O. Lundberg, M. Bodegård, L. Stolt, *Thin Solid Films* **2003**, *431*, 26.
- [61] M. Gloeckler, A. L. Fahrenbruch, J. R. Sites, “Numerical Modeling of CIGS and CdTe Solar Cells: Setting the Baseline,” *3rd World Conference on Photovoltaic Energy Conversion, 2003. Proceedings of, Osaka, 2003*, pp. 491–494.